

Variable Binding for Sparse Distributed Representations: Theory and Applications

E. Paxon Frady, Denis Kleyko, and Friedrich T. Sommer

Abstract—Symbolic reasoning and neural networks are often considered incompatible approaches in artificial intelligence. Connectionist models known as Vector Symbolic Architectures (VSAs) can potentially bridge this gap by enabling symbolic reasoning with distributed representations (Plate, 1994; Gayler, 1998; Kanerva, 1996). However, classical VSAs and neural networks are still incompatible because they represent information differently. VSAs encode symbols by dense pseudo-random vectors, where information is distributed throughout the entire neuron population. Neural networks encode features locally, by the activity of single neurons or small groups of neurons, often forming sparse vectors of neural activation (Hinton et al., 1986). Following Rachkovskij (2001); Laiho et al. (2015), we explore symbolic reasoning with sparse distributed representations.

The core operations in VSAs are dyadic operations between vectors to express variable binding and the representation of sets. Thus, algebraic manipulations enable VSAs to represent and process data structures of varying depth in a vector space of fixed dimensionality. Using techniques from compressed sensing, we first show that variable binding between dense vectors in classical VSAs (Gayler, 1998) is mathematically equivalent to tensor product binding (Smolensky, 1990) between sparse vectors, an operation which increases dimensionality. This theoretical result implies that dimensionality-preserving binding for general sparse vectors must include a reduction of the tensor matrix into a single sparse vector.

Two options for sparsity-preserving variable binding are investigated. One binding method for general sparse vectors extends earlier proposals to reduce the tensor product into a vector, such as circular convolution (Plate, 1994). The other variable binding method is only defined for sparse block-codes (Gripon and Berrou, 2011), block-wise circular convolution (Laiho et al., 2015). Our experiments reveal that variable binding for block-codes has ideal properties, whereas binding for general sparse vectors also works, but is lossy, similar to previous proposals (Rachkovskij, 2001). We demonstrate a VSA with sparse block-codes in example applications, cognitive reasoning and classification, and discuss its relevance for neuroscience and neural networks.

Index Terms—vector symbolic architectures, compressed sensing, tensor product variable binding, sparse distributed representations, sparse block-codes, cognitive reasoning, classification

I. INTRODUCTION

In a traditional computer, the internal representation of data is organized by data structures. A data structure is a collection of data values with their relationships. For example, a simple data structure is a key-value pair, relating a variable name to its assigned value. Particular variables within data structures can be

individually accessed for computations. Data structures are the backbones for computation, and needed for organizing, storing, managing and manipulating information in computers.

For many tasks that brains have to solve, for instance analogical inference in cognitive reasoning tasks and invariant pattern recognition, it is essential to represent knowledge in data structures and to query the components of data structures on the fly. It has been a long-standing debate if, and if so how, brains can represent data structures with neural activity and implement algorithms for their manipulation (Fodor et al., 1988).

Here, we revisit classical connectionist models (Plate, 1994; Kanerva, 1996; Gayler, 1998) that propose encodings of data structures with distributed representations. Following Gayler (2003), we will refer to these models as *Vector Symbolic Architectures* (VSAs), synonymously their working principles are sometimes summarized as *hyperdimensional computing* (Kanerva, 2009). Typically, VSA models use dense random vectors to represent atomic symbols, such as variable names and feature values. Atomic symbols can be combined into compound symbols that are represented by vectors that have the same dimension. The computations with pseudo-random vectors in VSAs rest on the concentration of measure phenomenon (Ledoux, 2001) that random vectors become almost orthogonal in large vector spaces (Frady et al., 2018).

In neural networks, features are encoded locally by the activity of a single or of a few neurons. Also, patterns of neural activity are often sparse, i.e. there are only few nonzero elements (Willshaw et al., 1969; Olshausen and Field, 1996). Connectionists attempted to use such local feature representations in models describing computations in the brain. However, a critical issue emerged with these representations, known as *the binding problem* in neuroscience. This problem occurs when a representation requires the encoding of sets of feature conjunctions, for example when representing a red triangle and a blue square (Treisman, 1998). Just representing the color and shape features would lose the binding information that the triangle is red, not the square. One solution proposed for the binding problem is the tensor product representation (TPR) (Smolensky, 1990), where a neuron is assigned to each combination of feature conjunctions. However, when expressing hierarchical data structures, the dimensionality of TPRs grows exponentially with hierarchical depth. One proposal to remedy this issue is to form reduced representations of TPRs, so that the resulting representations have the same dimensions as the atomic vectors (Hinton et al., 1990; Plate, 1993). This has been the inspiration of VSAs, which have proposed various algebraic operations for binding that preserve dimensionality. Building on

E. P. Frady and F. T. Sommer are with Neuromorphic Computing Lab, Intel Labs and also with the Redwood Center for Theoretical Neuroscience at the University of California, Berkeley, CA 94720, USA.

D. Kleyko is with the Redwood Center for Theoretical Neuroscience at the University of California, Berkeley, CA 94720, USA and also with Intelligent systems Lab at Research Institutes of Sweden, 164 40 Kista, Sweden.

earlier work on sparse VSA (Rachkovskij, 2001; Laiho et al., 2015), we investigate the possibility to build binding operations for sparse patterns that preserve dimensionality and sparsity.

The paper is organized as follows. In section II, the background for our study is introduced, which covers different flavors of symbolic reasoning, sparse distributed representations, and the basics of compressed sensing. In section III-A, compressed sensing is employed to establish the equivalence between the dense representations in classical VSA models and sparse representations. This treatment reveals the operations between sparse vectors that are induced by VSA operations defined on dense vectors. Interestingly, we find that the classical dimensionality-preserving operations in VSAs induce equivalent operations between sparse vectors that do not preserve dimensionality. Section III-B introduces and investigates concrete methods for dimensionality- and sparsity-preserving variable binding. Known binding methods, such as circular convolution (Plate, 1994) and vector-derived transformation binding (Gosmann and Eliasmith, 2019), lead to binding operations that are dimensionality- but not sparsity-preserving. We investigate two solutions for sparsity-preserving binding, one for general sparse vectors, and one for the subset of sparse block vectors (block-codes). Section III-C demonstrates the most promising solution, a VSA with sparse block-codes in two applications. In Section IV, we summarize our results and discuss their implications.

II. BACKGROUND

A. Models for symbolic reasoning

Many connectionist models for symbolic reasoning with vectors use vector addition (or a thresholded form of it) to express sets of symbols. But the models characteristically deviate in encoding strategies and in their operation for binding. TPRs (Smolensky, 1990) use real-valued localist feature vectors $\mathbf{x}, \mathbf{y} \in \mathbb{R}^N$ and the outer product $\mathbf{x} \mathbf{y}^\top \in \mathbb{R}^{N \times N}$ as the binding operation. This form of tensor product binding encodes compound data structures by representations that have higher dimensions than those of atomic symbols. The deeper a hierarchical data structure, the higher the order of the tensor.

Building on Hinton’s concept of reduced representations (Hinton, 1990), several VSA models were proposed (Plate, 1994; Kanerva, 1996; Gayler, 1998) in which atomic and composed data structures have the same dimension. These models encode atomic symbols by pseudo-random vectors and the operations for set formation and binding are designed in a way that representations of compound symbols still resemble random vectors. The operations for *addition* (+) and *binding* (\circ) are dyadic operations that form a ring-like structure. The desired properties for a binding operation are:

- i) Associative, i.e., $(\mathbf{a} \circ \mathbf{b}) \circ \mathbf{c} = \mathbf{a} \circ (\mathbf{b} \circ \mathbf{c}) = (\mathbf{a} \circ \mathbf{c}) \circ \mathbf{b}$.
- ii) Distributes over addition, i.e., $\sum_i^{D_1} \mathbf{a}^i \circ \sum_j^{D_2} \mathbf{b}^j = \sum_{i,j}^{D_1, D_2} \mathbf{c}^{ij}$ with $\mathbf{c}^{ij} = \mathbf{a}^i \circ \mathbf{b}^j$.
- iii) Has an inverse operation to perform unbinding.

Holographic Reduced Representation (HRR) (Plate, 1991, 1995) was probably the earliest formalized VSA which uses real-valued Gaussian random vectors and circular convolution

as the binding operation. Circular convolution is the standard convolution operation used in the discrete finite Fourier transform which can be used to produce a vector from two input vectors \mathbf{x} and \mathbf{y} :

$$(\mathbf{x} \circ \mathbf{y})_k := (\mathbf{x} * \mathbf{y})_k = \sum_{i=1}^N x_{(i-k) \bmod N} y_i \quad (1)$$

Other VSA models use binding operations based on projections of the tensor product matrix that only sample the matrix diagonal. For example, the *Binary Spatter Code (BSC)* (Kanerva, 1996) uses binary random vectors and binding is the XOR operation between components with the same index.

In the following, we focus on the *Multiply-Add-Permute (MAP) model* (Gayler, 1998), which uses bipolar atomic vectors whose components are -1 and 1. Atomic features or symbols are represented by random vectors of a matrix Φ , called the *codebook*. The columns of Φ are normalized i.i.d. random *code vectors*, $\Phi_i \in \{\pm 1\}^N$. The binding operation is the Hadamard product between the two vectors:

$$\mathbf{x} \circ \mathbf{y} := \mathbf{x} \odot \mathbf{y} = (x_1 y_1, x_2 y_2, \dots, x_N y_N)^\top \quad (2)$$

When the binding involves just a scalar value, the multiplication operation (2) relaxes to ordinary vector-scalar multiplication. A feature with a particular value is simply represented by the vector representing the feature, Φ_i (which acts like a “key”), multiplied with the scalar representing the “value” a_i : $\mathbf{x} = \Phi_i a_i$.

For representing a *set of features*, the generic vector addition is used, and the vector representing a set of features with specific values is then given by:

$$\mathbf{x} = \Phi \mathbf{a} \quad (3)$$

Here, the nonzero components of \mathbf{a} represent the values of features contained in the set, the zero-components label the features that are absent in the set.

Although the representation \mathbf{x} of this set is lossy, a particular feature value can be approximately decoded by forming the inner product with the corresponding “key” vector:

$$a_i \approx \Phi_i^\top \mathbf{x} / N, \quad (4)$$

where N is the dimension of vectors. The cross-talk noise in the decoding (4) decreases with the square root of the dimension of the vectors or by increasing the sparseness in \mathbf{a} , for analysis of this decoding procedure, see (Fraday et al., 2018).

To represent a set of sets, one cannot simply form a sum of the compound vectors. This is because a feature binding problem occurs, and the set information on the first level is lost. VSAs can solve this issue by combining addition and binding to form a representation of a set of compound objects in which the integrity of individual objects is preserved. This is sometimes called the *protected sum* of L objects:

$$\mathbf{s} = \sum_j^L \Psi_j \odot \mathbf{x}^j \quad (5)$$

where Ψ_j are dense bipolar random vectors that label the different compound objects. Another method for representing

protected sums uses powers of a single random permutation matrix \mathbf{P} (Laiho et al., 2015; Frady et al., 2018):

$$\mathbf{s} = \sum_j^L (\mathbf{P})^{(j-1)} \mathbf{x}^j \quad (6)$$

In general, algebraic manipulation in VSAs yields a noisy representation of the result of a symbolic reasoning procedure. To filter out the result, so-called *cleanup memory* is required, which is typically nearest-neighbor search in a content-addressable memory or associative memory (Willshaw et al., 1969; Palm, 1980; Hopfield, 1982) storing the codebook(s).

B. Sparse distributed representations

The classical VSAs described in the previous section use dense representations, that is, vectors in which most components are nonzero. In the context of neuroscience and neural networks for unsupervised learning and synaptic memory, another type of representation has been suggested: *sparse representations*. In sparse representations, a large fraction of components are zero, e.g. most neurons are silent. Sparse representations capture essential aspects of receptive field properties seen in neuroscience when encoding sensory inputs, such as natural images or natural sound (Olshausen and Field, 1996; Bell and Sejnowski, 1997).

Here, we will investigate how sparse representations can be used in VSAs. For the cleanup required in VSAs, sparse representations have the advantage that they can be stored more efficiently than dense representations in Hebbian synapses (Willshaw et al., 1969; Palm, 1980; Tsodyks and Feigl'man, 1988; Palm and Sommer, 1992; Frady and Sommer, 2019). However, how the algebraic operations in VSAs can be performed with sparse vectors has only been addressed in a few previous studies (Rachkovskij, 2001; Laiho et al., 2015).

A particular type of sparse representation with additional structure has been proposed for symbolic reasoning before: *sparse block-codes* (Laiho et al., 2015). In a K -sparse block-code, the ratio between active components and total number of components is K/N , as usual. But the index set is partitioned into K blocks, each block of size N/K , with one active element in each block. Thus, the activity in each block is maximally sparse, it only contains a single nonzero component¹.

The constraint of a sparse block-code reduces the entropy in a code vector significantly, from $\log \binom{N}{K}$ to $K \log \left(\frac{N}{K}\right)$ bits (Gritsenko et al., 2017). At the same time, the block constraint can also be exploited to improve the retrieval in Hebbian associative memory. As a result, the information capacity of associative memories with Hebbian synapses for block-coded sparse vectors is almost the same as for unconstrained sparse vectors (Gripon and Berrou, 2011; Knoblauch and Palm, 2020). Sparse block-codes also may reflect coding principles observed in the brain, such as competitive mechanisms between sensory neurons representing different features (Heeger, 1992), as well

¹Note that sparse block-codes differ from sparse block signals (Eldar et al., 2010), in the latter the activity within blocks can be non-sparse but the nonzero blocks is K' -sparse, with $K' \ll K$. The resulting N -dimensional vectors have a ratio between active components and total number of components of $K'L/N = K'/K$.

as orientation hypercolumns seen in the visual system of certain species (Hubel and Wiesel, 1977).

Recent proposals also include sparse phasor-codes for representing information, where the active elements in the population are not binary, but complex-valued with binary magnitudes and arbitrary phases (Frady and Sommer, 2019). Such a coding scheme may be relevant for neuroscience, as they can be represented with spikes and spike-timing. VSA architectures have also been demonstrated in the complex domain (Plate, 2003), which use dense vectors of unit-magnitude phasors as atomic symbols. Here, we also propose and analyze a variation of the block-code where active entries are phasors.

C. Compressed sensing

Under certain conditions, there is unique equivalence between sparse and dense vectors that has been investigated under the name *compressed sensing* (CS) (Candes et al., 2006; Donoho et al., 2006). Many types of measurement data, such as images or sounds, have a sparse underlying structure and CS can be used as a compression method, in applications or even for modeling communication in biological brains (Hillar and Sommer, 2015). For example, if one assumes that the data vectors are K -sparse, that is:

$$\mathbf{a} \in \mathcal{A}_K := \{\mathbf{a} \in \mathbb{R}^M : \|\mathbf{a}\|_0 \leq K\} \quad (7)$$

with $\|\cdot\|_0$ the L0-norm. In CS, the following linear transformation creates a dimensionality-compressed dense vector from the sparse data vector:

$$\mathbf{x} = \mathbf{\Xi} \mathbf{a} \quad (8)$$

where $\mathbf{\Xi}$ is a $N \times M$ random sampling matrix, with $N < M$.

Due to the distribution of sparse random vectors \mathbf{a} , the statistics of the dimensionality-compressed dense vectors \mathbf{x} becomes somewhat non-Gaussian. The data vector can be recovered from the compressed vector \mathbf{x} by solving the following sparse inference problem:

$$\hat{\mathbf{a}} = \operatorname{argmax}_{\mathbf{a}} (\mathbf{x} - \mathbf{\Xi} \mathbf{a})^2 + \lambda \|\mathbf{a}\|_1 \quad (9)$$

The condition for K , N , M and $\mathbf{\Xi}$, under which the recovery (9) is possible, forms the cornerstones of compressed sensing (Donoho et al., 2006; Candes et al., 2006).

For CS to work, a necessary condition is that the sampling matrix is injective for the sparse data vectors, i.e. that the intersection between the kernel of the sampling matrix, $\operatorname{Ker}(\mathbf{\Xi}) = \{\mathbf{a} : \mathbf{\Xi} \mathbf{a} = 0\}$, with the set of sparse data vectors, \mathcal{A}_K , is empty: $\operatorname{Ker}(\mathbf{\Xi}) \cap \mathcal{A}_K = \emptyset$. But, this condition does not guarantee that each data vector has a unique dense representation. In other words, the mapping between data vectors and dense representations must also be bijective. To guarantee uniqueness of the dense representation of K -sparse vectors, the kernel of the sampling matrix must not contain any $(2K + 1)$ -sparse vector:

$$\operatorname{Ker}(\mathbf{\Xi}) \cap \mathcal{A}_{2K+1} = \emptyset \quad (10)$$

with \mathcal{A}_{2K+1} being the set of $(2K+1)$ -sparse vectors. Intuitively, the condition (10) excludes that any two K -sparse data vectors

can have the same dense representation: $\mathbf{a}_1 \neq \mathbf{a}_2$: $\Xi \mathbf{a}_1 - \Xi \mathbf{a}_2 = 0$.

Even with condition (10), it still might not be possible to infer the sparse data vectors from the dense representations (9) in the presence of noise. Another common criterion for CS to work is the s -restricted isometry property (RIP):

$$(1 - \delta_s) \|\mathbf{a}^s\|_2^2 \leq \|\Xi \mathbf{a}^s\|_2^2 \leq (1 + \delta_s) \|\mathbf{a}^s\|_2^2 \quad (11)$$

with the vector \mathbf{a}^s s -sparse, and the RIP constant $\delta_s \in (0, 1)$. The choice $\delta_{2K+1} = 1$ is equivalent to condition (10). With a choice $\delta_{2K+1} = \delta^* < 1$, one can impose a more stringent condition that enables the inference, even in the presence of noise. The minimal dimension of the compression vector that guarantees (11) is typically linear in K but increases only logarithmically with M :

$$N \geq C K \log \left(\frac{M}{K} \right) \quad (12)$$

where C is a constant of order $O(1)$ that depends on δ_{2K+1} . Here, we will use the uniqueness conditions (10) and (11) to assess the equivalence between different models of symbolic reasoning.

III. RESULTS

A. Equivalent representations with sparse vs. dense vectors

In this section, we consider a setting where sparse and dense symbolic representations can be directly compared. Specifically, we ask what operations between K -sparse vectors are induced by the operations in the MAP VSA. To address this question, we map K -sparse feature vectors to corresponding dense vectors via (3). The column vectors of the codebook in (3) correspond to the atomic dense vectors in the VSA. We choose the dimension N and properties of the codebook(s) and sparse random vectors so that the CS condition (10) is fulfilled². Thus, each sparse vector has a unique dense representation and vice versa.

1) *Improved VSA decoding based on CS*: In our setting, the coefficient vector \mathbf{a} is sparse. The standard decoding method in VSA (4) provides a noisy estimate of the sparse vector (Fig. 1) from the dense representation. However, if the sparse vector and the codebook Φ in (3) satisfy the compressed sensing conditions, one can do better: decoding à la CS (9) achieves near-perfect accuracy (Fig. 1). Note that sparse inference requires that the entire coefficient vector \mathbf{a} is decoded at once, similar to Ganguli and Sompolinsky (2010), while with (4) individual values a_i can be decoded separately. If the CS condition is violated, sparse inference (9) abruptly ceases to work, while the VSA decoding with (4) gradually degrades, see Frady et al. (2018).

²In compressed sensing, the choice of sampling matrices with binary or bipolar random entries is common, e.g. (Amini and Marvasti, 2011).

2) *Variable binding operation*: The Hadamard product between dense vectors turns out to be a function of the tensor product, i.e. the TPR, of the corresponding sparse vectors:

$$\begin{aligned} (\mathbf{x} \odot \mathbf{y})_i &= (\Phi \mathbf{a})_i (\Psi \mathbf{b})_i = \sum_l \Phi_{il} a_l \sum_k \Psi_{ik} b_k \\ &= \sum_{lk} \Phi_{il} \Psi_{ik} a_l b_k = ((\Phi \square \Psi) \text{vec}(\mathbf{a} \mathbf{b}^\top))_i \end{aligned} \quad (13)$$

This linear relationship between the Hadamard product of two vectors and the TPR can be seen as a generalization of the Fourier convolution theorem, see Appendix A.

The reshaping of the structure on the RHS of (13) also shows that there is a relationship to the matrix vector multiplication in CS sampling (8): The ravelled tensor product matrix of the sparse vectors becomes a M^2 -dimensional vector $\text{vec}(\mathbf{a} \mathbf{b}^\top)$ with K^2 nonzero elements. Further, $(\Phi \square \Psi)$ is a $N \times M^2$ sampling matrix, formed by pair-wise Hadamard products of vectors in the individual dictionaries Φ and Ψ :

$$(\Phi \square \Psi) := (\Phi_1 \odot \Psi_1, \Phi_1 \odot \Psi_2, \dots, \Phi_M \odot \Psi_M) \quad (14)$$

One can now ask under what conditions Hadamard product and tensor product become mathematically equivalent, that is, can any sparse tensor product in (13) be uniquely inferred from the Hadamard product using a CS inference procedure (9). The following two lemmas consider a worst-case scenario in which there is equivalence between the atomic sparse and dense vectors, which requires that the sparks of the individual codebooks are at least $2K + 1$.

Lemma 1: Let $\text{Spark}(\Phi) = \text{Spark}(\Psi) = 2K + 1$. Then the spark of the sampling matrix in (13) is $\text{Spark}((\Phi \square \Psi)) \leq 2K + 1$.

Proof: Choose a $(2K + 1)$ -sparse vector \mathbf{c} in the kernel of Φ , and choose any cardinal vector $\mathbf{b}^j := (0, \dots, 0, 1, 0, \dots, 0)$ with the nonzero component at index j . Then we have: $0 = \Phi \alpha = \Phi \mathbf{c} \odot \Psi_j = \sum_{i \in \alpha} c_i \Phi_i \odot \Psi_j = (\Phi \square \Psi) \text{vec}(\mathbf{c} \otimes \mathbf{b}^j)$. Thus the $(2K + 1)$ -sparse vector $\text{vec}(\mathbf{c} \otimes \mathbf{b}^j)$ lies in the kernel of the sampling matrix in (13). There is also a small probability that the construction of $(\Phi \square \Psi)$ produces a set of columns with less than $2K + 1$ components that are linearly dependent. \square

Lemma 1 reveals that the sampling matrix (14) does certainly not allow the recovery of K^2 -sparse patterns in general. However, this is not required since the reshaped outer products of K -sparse vectors form a subset of K^2 -sparse patterns. The following lemma shows that for this subset recovery can still be possible.

Lemma 2: The difference between the outer-products of pairs of K -sparse vectors cannot fully coincide in support with the $(2K + 1)$ -sparse vectors in the kernel of the sampling matrix of (13) as identified by Lemma 1. Thus, although $\text{Spark}((\Phi \square \Psi)) \leq 2K + 1$, the recovery of reshaped tensor products from the Hadamard product can still be possible.

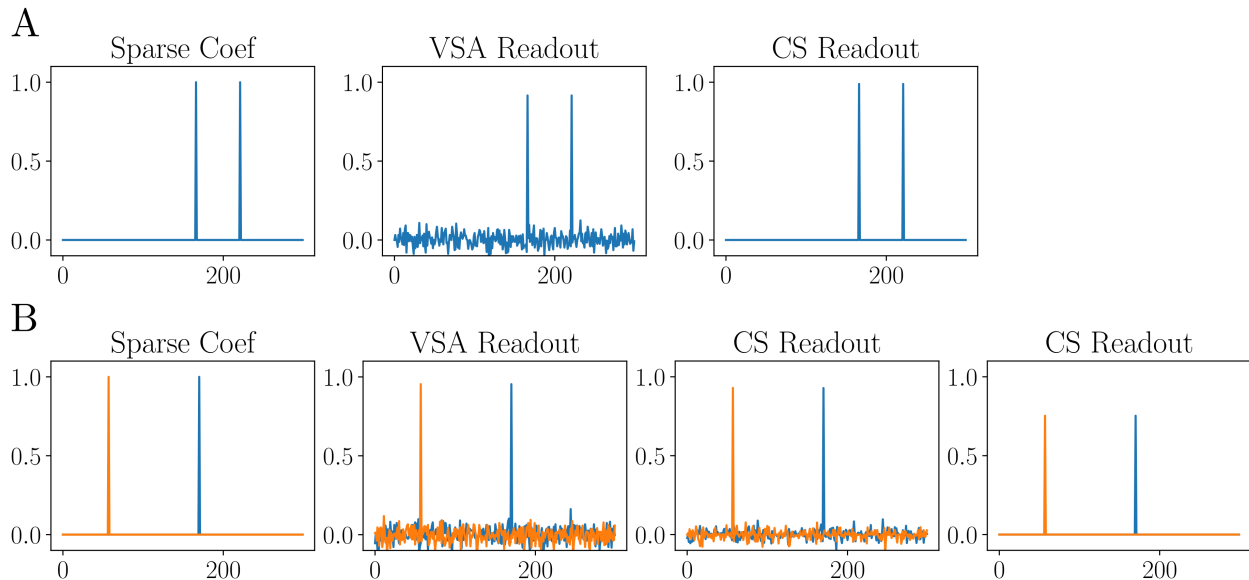


Fig. 1. **Readout of sparse coefficients from dense distributed representation.** A. The sparse coefficients (left) are stored as a dense representation using a random codebook. The coefficients are recovered with standard VSA readout (middle) and with sparse inference (right), which reduces the crosstalk noise. B. Two sparse coefficients are stored as a protected set (left). Readout with sparse inference reduces crosstalk noise, but some noise can remain depending on sparsity penalty.

Proof: The $(2K+1)$ -sparse vectors in the kernel of the sampling matrix $(\Phi \boxtimes \Psi)$ identified in Lemma 1 correspond to an outer product of a $(2K+1)$ -sparse vector with a 1-sparse vector. The resulting matrix has $2K+1$ nonzero components in one single column.

The difference of two outer products of K -sparse vectors yields a matrix which can have maximally $2K$ nonzero components in one column. Thus, the sampling matrix should enable the unique inference of the tensor product from the Hadamard product of the dense vectors.

□

Lemmas 1 and 2 investigate the equivalence of Hadamard and tensor product binding in the worst case, that is, when the codebooks have the minimum spark that still guarantees the unique equivalence between the sparse and dense atomic vectors. To explore the equivalence in the case of random codebooks, we performed simulation experiments with a large ensemble of randomly generated codebook pairs (Φ, Ψ) . Fig. 2 shows the averaged worst (i.e., highest) RIP constant amongst the ensembles for inferring the tensor product from the Hadamard product (solid red line).

Compared to the RIP constant for inferring the sparse representations of atomic vectors (black line), the RIP constant for inferring the tensor product (red line) is significantly higher. Thus, tensor product and Hadamard product are not always equivalent even if the atomic sparse and dense vectors are equivalent – in the example, when the dimension of dense vectors is between $N = 40$ to $N = 140$. However, with the dimension of dense vectors large enough ($N > 140$), the equivalence holds. Further, the controls in Fig. 2 help to explain the reasons for the gap in equivalence for small dense vectors.

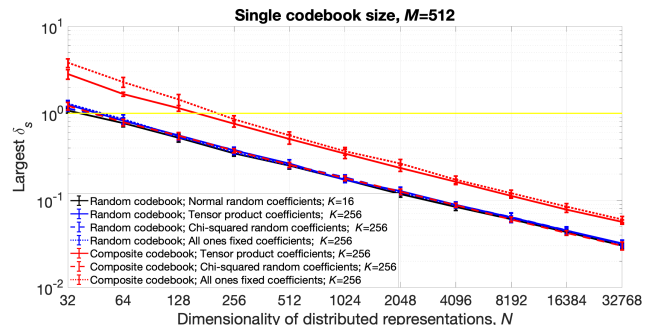


Fig. 2. **Worst-case RIP constant for inferring sparse tensor products in ensemble of random codebooks.** The largest empirical RIP constant (δ_s) in an ensemble of 10 pairs of pseudo-random dictionaries Φ, Ψ . For each pair the maximum RIP was determined by compressing 10000 sparse vectors. For successful inference of the sparse representations, the RIP constant has to be below the $\delta_s = 1$ level (yellow line). The black solid line represents the RIP for inferring atomic sparse vectors from dense vectors formed according to (8). The red solid line represents the RIP for inferring tensor products from dense vectors formed according to (13). Other lines in the diagram are controls. The blue solid line represents the RIP for a $(N \times M^2)$ random dictionary in which all elements are independently sampled rather than constructed by $\Phi \boxtimes \Psi$ from the smaller dictionaries. Dashed and dotted red lines represent the RIP using the $\Phi \boxtimes \Psi$ sampling matrix with sparse vectors with independent random components, rather than formed by a tensor product $\text{vec}(\mathbf{a} \mathbf{b}^T)$ of two random vectors. The blue dashed line is for real-valued vectors with elements sampled from a Chi-squared distribution, the blue dotted line for binary random vectors. Dashed and dotted blue lines represent the RIP for the same type of independent random vectors with the independent random sampling matrix.

The RIP constants are significantly reduced if the tensor product is subsampled with a fully randomized matrix (solid blue line), rather than with the sampling matrix resulting from (13). In contrast, the requirement to infer outer products of continuous valued random vectors (solid red line) does not much increase the RIP values over the RIP requirement for the inference of

outer products of binary vectors (dotted red line). Thus, we conclude that sampling with matrix $\Phi \square \Psi$ (14), which is not i.i.d. random but formed by a deterministic function from the smaller atomic random sampling matrices, requires a somewhat bigger dimension of the dense vectors to be invertible.

Here we have shown that under certain circumstances the binding operation between dense vectors in the MAP VSA is mathematically equivalent to the tensor product between the corresponding sparse vectors. This equivalence reveals a natural link between two prominent proposals for symbolic binding in the literature, the dimensionality preserving binding operations in VSA models, with the tensor product in the TPR model (Smolensky, 1990; Smolensky et al., 2016). In other VSA models, such as HRR (Plate, 2003), atomic symbols are represented by dense Gaussian vectors and the binding operation is circular convolution. Our treatment can be extended to these models by simply noting that by the Fourier convolution theorem (28) circular convolution is equivalent to the Hadamard product in the Fourier domain, i.e. $\mathbf{x} * \mathbf{y} = \mathcal{F}^{-1}(\mathcal{F}(\mathbf{x}) \odot \mathcal{F}(\mathbf{y}))$.

3) *Set operations*: Summing dense vectors corresponds to summing the sparse vectors

$$\mathbf{x} + \mathbf{y} = \Phi(\mathbf{a} + \mathbf{b}) \quad (15)$$

Thus, the sum operation represents a bag of features from all objects, but the grouping information on how these features were configured in the individual objects is lost. The inability to recover the individual compound objects from the sum representation has been referred to as the binding problem in neuroscience (Treisman (1998)).

The protected sum of set vectors (5) can resolve the binding problem. This relies on binding the dense representations of the individual objects to a set of random vectors that act as keys, stored in the codebook Ψ (5):

$$\sum_j^L \Psi_j \odot \mathbf{x}^j = \sum_j^L \Psi_j \odot \sum_i^M \Phi_i a_i^j = (\Phi \square \Psi)(\mathbf{a}^1, \mathbf{a}^2, \dots, \mathbf{a}^L) \quad (16)$$

This shows that the protected sum can be computed from the concatenation of sparse vectors. The concatenation of sparse vectors is a representation that fully contains the binding information, but again leads to an increase in dimensionality. Similar to (13), (16) describes linear sampling of a sparse vector like in compressed sensing. The sampling matrix $(\Phi \square \Psi)$ is a $N \times ML$ sampling matrix formed by each pair of vectors in Φ and Ψ , as in (14), and the sparse vector is the ML -dimensional concatenation vector.

We again ask under what conditions the sparse concatenation vector can be uniquely inferred given the dense representation of the protected sum, which makes the dense and sparse representations equivalent. Like in section III-A2, we first look at the worst case scenario, and then perform an experiment with codebooks composed of random vectors. The worst case scenario assumes the spark of Φ to be $2K+1$, just big enough that atomic vectors can be inferred uniquely. By Lemma 1, the spark of the sampling matrix is smaller or equal to $2K+1$, smaller than the sparsity KL of vectors to be inferred. Again, the vectors to be inferred are a subset of KL -sparse vectors, the vectors that have K

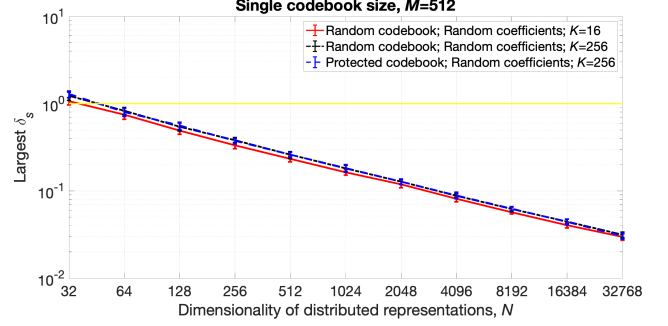


Fig. 3. **Worst-case RIP constant for inferring sparse representations of protected sums in ensemble of random codebooks.** The largest empirical RIP constant (δ_s) in ensemble of 10 pairs of pseudo-random dictionaries Φ, Ψ . For each pair the maximum RIP was determined by compressing 10000 sparse vectors. For successful inference of the sparse representations, the RIP constant has to be below the $\delta_s = 1$ level (yellow line). Red solid line represents RIP values for inferring atomic sparse vectors from dense vectors formed according to (8). Blue dashed line represents RIP values for inferring protected sum from dense vectors formed according to (16). For comparison, black dotted line represents RIP values for inferring protected sum when instead of $\Phi \square \Psi$ the dictionary is random.

nonzero components in each of the L M -sized compartments. Thus, as in Lemma 2 for the Hadamard product, the difference formed by two of these vectors can maximally produce $2K$ nonzero components in each compartment, and therefore never coincide with a kernel vector of the sampling matrix.

Fig. 3 shows the results of simulation experiments with an ensemble of random codebooks. For the protected sum, the worst RIP values of the inference of individual sparse vectors versus the list of sparse vectors composing the protected sum do coincide. Thus, the dense protected sum vector and the list of sparse feature vectors are equivalent.

The alternative method of forming a protected sum (6) using powers of a permutation matrix \mathbf{P} , corresponds equally to a sampling of the concatenation of the sparse vectors. As long as the sampling matrices $(\Phi, \mathbf{P}\Phi, \mathbf{P}^2\Phi, \dots, \mathbf{P}^{(L-1)}\Phi)$ and $(\Phi \square \Psi)$ have similar properties, the conditions for equivalence between protected sum and concatenated sparse vectors hold.

B. Dimension- and sparsity-preserving VSA operations

The results from Sect. III-A reveal that variable binding and the protected set representation in classical VSA models induce equivalent operations between sparse vectors that are not dimensionality preserving. Thus, dimensionality-preserving operations for binding and protected sum involve potentially lossy transformations of the higher dimensional data structure into a single vector. However, dimensionality-preserving binding operations have only been defined for dense VSA representations. In the following, we investigate binding operations on sparse VSA representations that are both dimensionality- and sparsity-preserving, one for general sparse vectors and one for sparse vectors with block structure.

1) *Sparsity-preserving binding for general K -sparse vectors*: Binding operations in VSAs can all be described as a projection of the tensor product to a vector, including Hadamard product, circular convolution binding (Plate, 2003) and vector-

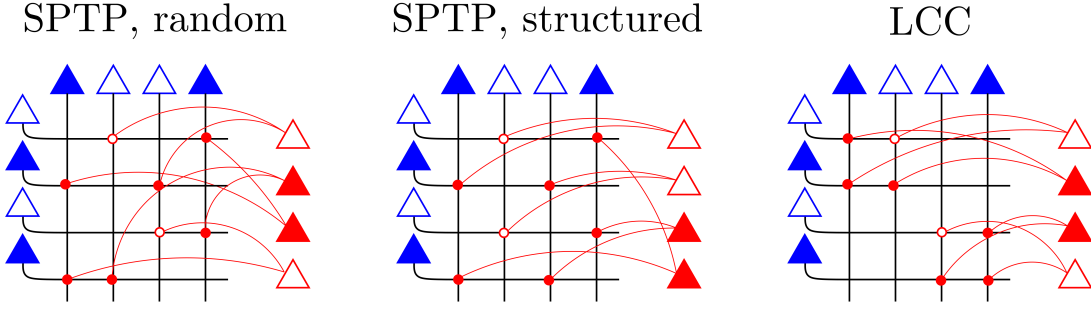


Fig. 4. **Circuits for sparsity-preserving binding:** Three pools of neurons (blue: two inputs, red: output) represent the sparse neural activity patterns **a**, **b** and **c**. The dendritic tree of the output neurons contains coincidence detectors that detect pairs of co-active axons (red circles), and the soma (red triangles) sums up several coincidence detectors based on the required fan-in. Each neuron samples only a subset of the outer product depending on the desired sparsity and threshold settings. The subsampling pattern of neurons is described by a binary tensor $W_{ij}^l \in \{0, 1\}$, where i, j indexes the coincidence point and l the postsynaptic neuron. We examine three different sampling strategies random sampling, structured sampling, and the block-code.

derived transformation binding (VDTB) (Gosmann and Eliasmith, 2019), see Appendix (26). However, when applied to sparse atomic vectors, these operations do not preserve sparsity – circular convolution produces a vector with reduced sparsity, while the Hadamard product increases sparsity.

Ideally, a sparsity-preserving VSA binding operation operates on two atomic vectors that are K -sparse and produces a K -sparse vector that has the correct algebraic properties. To preserve sparsity, we developed a binding operation that is a projection from a sub-sampling of the tensor product. We refer to this operation as *sparsity-preserving tensor projection (SPTP)*. Given two K -sparse binary vectors **a** and **b**, SPTP variable binding is given by:

$$(\mathbf{a} \circledast \mathbf{b})_l = H \left(\sum_{ij} W_{ij}^l a_i b_j - \theta \right) \quad (17)$$

Here $H(x)$ is the Heaviside function, θ is a threshold. For a pair of K -sparse complex phasor vectors, SPTP binding is defined as:

$$\begin{aligned} (\mathbf{a} \circledast \mathbf{b})_l &= \frac{z_l}{|z_l|} H(|z_l| - \theta) \\ z_l &= \sum_{ij} W_{ij}^l a_i b_j \end{aligned} \quad (18)$$

The computation of (17) resembles a circuit of threshold neurons with coincidence detectors in their dendritic trees, see Fig. 4. The synaptic tensor $\mathbf{W} \in \{0, 1\}^{M \times M \times M}$ is a binary third-order tensor that indicates how each output neuron samples from the outer-product. We examined two types of sampling tensors, one with the 1-entries chosen i.i.d. (without repetition), and one with 1-entries aligned along truncated diagonals of the tensor (left and middle panel in Fig. 4).

The sparsity of the output in (17) is controlled by the threshold and by the density of this sampling tensor. To achieve a target sparsity of K/N for a threshold $\theta = 1$, the fan-in to each neuron has to be N/K (see analysis in Appendix B-A). Thus, the minimal fan-in of the sampling tensor \mathbf{W} increases with sparsity. If the pattern activity is linear in the dimension, $K = \beta N$ with $\beta \ll 1$, the minimal fan-in is $\alpha^* = 1/\beta$.

In this case, the computational cost of SPTP binding is order N . If the pattern activity goes with the square root of the dimension, $K = \beta\sqrt{N}$, the minimal fan-in is $\alpha^* = \sqrt{N}/\beta$. If the pattern activity goes with the logarithm of the dimension, $K = \beta \ln(N)$, the minimal fan-in is $\alpha^* = N/(\beta \ln(N))$. Further, for optimizing the unbinding performance, the sampling tensor should fulfill the symmetry condition $W_{jl}^i = W_{ij}^l$ (see analysis in Appendix B-B).

2) *Sparsity-preserving binding for sparse block-codes:* We next consider sparse vector representations that are constrained as block-codes (Gripon and Berrou, 2011), which have been proposed for VSAs before (Laiho et al., 2015). Our model extends this previous work with a block-code in the complex domain. In a sparse block-code, a vector of length N is divided into K equally-sized blocks, each with a one-hot component. In the complex domain, the hot component is a phasor with unit amplitude and arbitrary phase.

The binding operation Laiho et al. (2015) proposed operates on each block individually. For each block, the indices of the two active elements of the input are summed modulo block size to produce the index for the active element of the output. This is the same as circular convolution (Plate, 1994) performed locally between individual blocks. This binding operation, *local circular convolution (LCC)*, denoted by $*_b$, produces a sparse block-code when the input vectors are sparse block-codes (Fig. 4). LCC variable binding can be implemented by forming the outer product and sampling as in Fig. 4, with a circuitry in which each neuron has a fan-in of $\alpha = N/K$ and samples along truncated diagonals of the tensor product. LCC has a computational complexity of αN , which is order N if K is proportional to N . An alternative implementation (that is more efficient on a CPU) uses the Fourier convolution theorem (28) to replace convolution by the Hadamard product:

$$\begin{aligned} (\mathbf{a} *_b \mathbf{b})_{block_i} &= \mathbf{a}_{block_i} *_b \mathbf{b}_{block_i} \\ &= \mathcal{F}^{-1} (\mathcal{F}(\mathbf{a}_{block_i}) \odot \mathcal{F}(\mathbf{b}_{block_i})) \end{aligned} \quad (19)$$

where \mathcal{F} is the Fourier transform.

The LCC unbinding of a block can be performed by computing the inverse of the input vector to unbind. This is the inverse

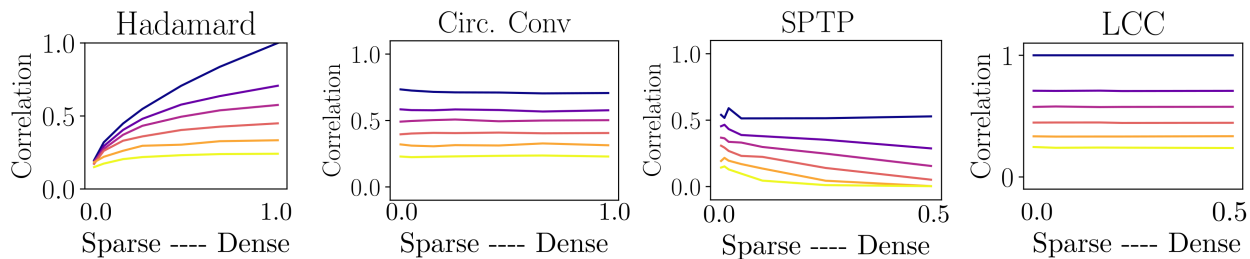


Fig. 5. **Comparison of binding operations.** The unbinding performance was measured as the correlation between ground truth and output of unbinding. Different levels of sparsity (x-axis) and superposition were examined (colored lines: [0, 1, 2, 4, 8, 16] items in superposition).

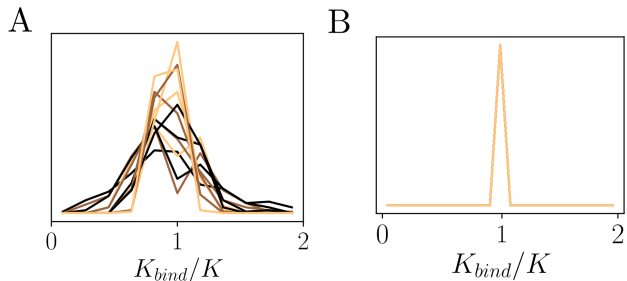


Fig. 6. **Preservation of sparsity with a binding operation.** A. The output sparsity K_{bind} is compared to the sparsity of the base vectors K . Binding with SPTP results in an output vector that has the correct expected sparsity, but there is some random variance. This variance reduces with more active components ($K = [20, 50, 100, 200]$ black to orange lines). This result is similar for both random and structured SPTP. B. The output sparsity of binding sparse block-codes with LCC deterministically results in a vector which maintains the sparsity of the inputs.

with respect to circular convolution, which is computed for each block,

$$\mathbf{a}_{block_i}^{-1} = \mathcal{F}^{-1}(\mathcal{F}(\mathbf{a}_{block_i})^*) \quad (20)$$

where $*$ is the complex conjugate. The inverse is used when unbinding, for instance, if $\mathbf{c} = \mathbf{a} *_b \mathbf{b}$, then $\mathbf{a} = \mathbf{b}^{-1} *_b \mathbf{c}$.

3) *Experiments with sparsity-preserving binding:* The binding operations are evaluated based on whether they maintain sparsity and how much information is retained when unbinding. Circular convolution and Hadamard product can be ruled out, because they do not preserve sparsity, the Hadamard product increases sparsity, and circular convolution reduces sparsity, but we still evaluated these operations for comparison.

We investigated how well sparsity is preserved with LCC and SPTP binding (Fig. 6). We find that LCC binding preserves sparsity perfectly, and SPTP binding preserves sparsity on average (statistically), but with some variance.

We next measure how much information is retained when first binding and then unbinding a vector using the proposed binding operations (Fig. 5). The Hadamard product binding achieves the highest correlation values for dense vectors, but performs very poorly for sparse vectors. The other three binding methods perform equally across sparsity levels. Circular convolution and SPTP binding are somewhat lossy for all sparsity levels. The LCC variable binding between block-codes achieves the highest correlation values, outperforming circular convolution,

and SPTP binding. Each diagram in Fig. 5 contains 6 curves, corresponding to different levels of additive superposition in the bound vectors.

SPTP binding works for general K -sparse vectors. It has decent properties but is somewhat lossy. The information loss is due to the fact that not all active input components contribute to the generation of active outputs, which means that some active input components cannot be inferred during unbinding and information is lost. The loss can be kept at a minimum by using a synaptic weight tensor that fulfills the symmetry condition $W_{jl}^i = W_{ij}^l$. This information loss persisted regardless of SPTP being structured or random, or the threshold and fan-in settings.

These experiments identify LCC binding as an ideal sparsity-preserving binding operation. With sparse block-codes and local circular convolution applied separately to each block, the unbinding is loss-less. The block structure guarantees that each active input component participates in the formation of an active output component, which cannot be guaranteed for general K -sparse vectors. Of course, there is a price to pay, LCC binding requires the atomic vectors to be sparse block-codes. The coding entropy of block-codes is significantly smaller than general K -sparse patterns.

C. Applications of VSAs with sparse block-codes

1) *Solving symbolic reasoning problems:* As a basic illustration of symbolic reasoning with sparse block-codes, we implement the solution to the cognitive reasoning problem (Kanerva, 2010): “What’s the dollar of Mexico?” in the supplemental Jupyter notebook. To answer such queries, data structures are encoded into vectors that represent trivia information about different countries. A data record of a country is a table of key-value pairs. For example, to answer the specific query, the relevant records are:

$$\begin{aligned} \text{ustates} &= \text{nam} *_b \text{usa} + \text{cap} *_b \text{wdc} + \text{cur} *_b \text{dol} \\ \text{mexico} &= \text{nam} *_b \text{mex} + \text{cap} *_b \text{mxc} + \text{cur} *_b \text{pes} \end{aligned}$$

The keys of the fields *country name*, *capital* and *currency* are represented by random sparse block-code vectors **nam**, **cap** and **cur**. The corresponding values *USA*, *Washington D.C.*, *Dollar*, *Mexico*, *Mexico City*, and *Peso* are also represented by sparse block-code vectors **usa**, **wdc**, **dol**, **mex**, **mxc**, **pes**. All the vectors are stored in the codebook Φ . The vectors **ustates**

and `mexico` represent the complete data records – they are a representation of key-value pairs that can be manipulated to answer queries. These record vectors have several terms added together, which reduces the sparsity.

To perform the reasoning operations required to answer the query, first the two relevant records have to be retrieved in the database. While `mexico` can be found by simple pattern matching between terms in the query and stored data record vectors, the retrieval of `ustates` is not trivial. The original work does not deal with the language challenge of inferring that the `ustates` record is needed. Rather, the problem is formally expressed as analogical reasoning, where the query is given as: *Dollar:USA::?:Mexico*. Thus, the pair of records needed for reasoning are given by the query.

Once the pair of records is identified, the following transformation vector is created:

$$\mathbf{t}_{UM} = \text{mexico} *_b \text{ustates}^{-1}$$

Note that unbinding with LCC is to bind with the inverse vector (20), whereas in the MAP VSA used in the original work (Kanerva, 2010) the binding and unbinding operations are the same. The transformation vector will also contain many summed terms, leading to less sparsity. The transformation vector then contains the relationships between the different concepts

$$\mathbf{t}_{UM} = \text{mex} *_b \text{usa}^{-1} + \text{mxc} *_b \text{wdc}^{-1} + \text{pes} *_b \text{dol}^{-1} + \text{noise}$$

where all of the cross-terms can be ignored and act as small amounts of cross-talk noise.

The correspondence to `dollar` can be computed by binding `dol` to the transformation vector:

$$\text{ans} = \text{dol} *_b \mathbf{t}_{UM} = \text{pes} + \text{noise}$$

The vector `ans` is then compared to each vector in the codebook Φ . The codebook entry with highest similarity represents the answer to the query. This will be *Peso* with high probability for large N . The probability of the correct answer can be understood through the capacity theory of distributed representations described in Frady et al. (2018), which we next apply to this context.

In general, a vector like \mathbf{t}_{UM} can be considered as a mapping between the fields in the two tables. The number of entries will determine the amount of crosstalk noise, but all of the entries that are non-sensible also are considered crosstalk noise.

Specifically, we consider general data records of key-value pairs, similar in form to `ustates` and `mexico`. These data records will contain R “role” vectors that act as keys. Each one has corresponding M_r potential “filler” values. The role vectors are stored in a codebook $\Psi \in \mathbb{C}^{N \times R}$. For simplicity, we assume that all R roles are present in a data record, each with one of the M_r fillers attached. The fillers for each role are stored in the codebook $\Phi^{(r)} \in \mathbb{C}^{N \times M_r}$. This yields a generic key-value data record:

$$\text{rec} = \sum_r^R \Psi_r *_b \Phi_{i^*}^{(r)} \quad (21)$$

where the index i^* indicates one filler vector from the codebook for a particular role.

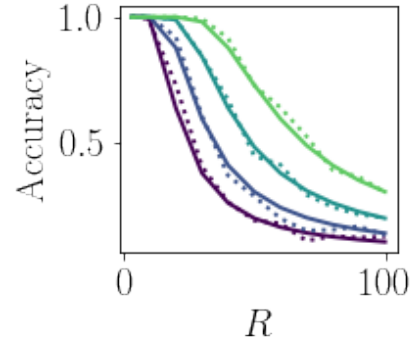


Fig. 7. **Performance of analogic reasoning tasks with sparse block-codes.** We empirically simulated analogic reasoning tasks with data records containing R key-value pairs, and measured the performance (dashed lines). This performance can be predicted based on the VSA capacity theory reported in Frady et al. (2018) (solid lines).

Next, we form the transformation vector, which is used to map one data record to another. This is done generically by binding two record vectors: $\mathbf{t}_{ij} = \text{rec}_j *_b \text{rec}_i^{-1}$.

As discussed, the terms in each record will distribute, and the values that share the same roles will be associated with each other. But, there are many cross-terms that are also present in the transformation vector that are not useful for any analogical reasoning query. The crosstalk noise is dependent on how many terms are present in the sum, and this includes the cross-terms. Thus, the total number of terms in the transformation vector \mathbf{t}_{ij} will be R^2 .

In the next step, a particular filler is queried and the result is decoded by comparison to the codebook Φ , which contains the sparse-block code of each possible filler:

$$\mathbf{a}_r = \Phi^{(r)}(\mathbf{t}_{ij} *_b \Phi_{j^*}^{(r)}) \quad (22)$$

where j^* indicates the index of the filler in the query (e.g. the index of *Dollar*). The entry with the largest amplitude in the vector \mathbf{a}_r is considered the output.

The probability that this inference finds the correct relationship can be predicted by the VSA capacity analysis (Frady et al., 2018) (Fig. 7). The probability is a function of the signal-to-noise ratio, given in this case by $s^2 = N/R^2$.

2) *Solving classification problems:* Although VSAs originated as models for symbolic reasoning, Kleyko et al. (2019) have recently described the similarities between VSAs and randomly connected feed-forward neural networks (Scardapane, S. and Wang, D., 2017) for classification, known as Random Vector Functional Link (RVFL) (Igel and Pao, 1995) or Extreme Learning Machines (ELM) (G. Huang and Q. Zhu and C. Siew, 2006). Specifically, RVFL/ELM can be expressed by VSA operations in the MAP VSA model (Kleyko et al., 2019). Leveraging these insights, we implemented a classification model using a VSA with sparse block-codes.

The model proposed in (Kleyko et al., 2019) forms a dense distributed representation \mathbf{x} of a set of features \mathbf{a} . Each feature is assigned a random “key” vector $\Phi_i \in \{\pm 1\}^N$. The collection of “key” vectors constitutes the codebook Φ . However, in contrast to (3) the set of features is represented differently. The

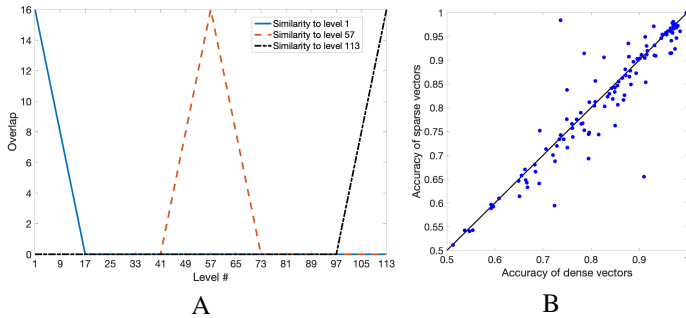


Fig. 8. **Solving classification problems with sparse block-codes.** A. Similarity preserving representation of scalars with sparse block-codes: $K = 16$, $N = 128$. Similarity (overlap) between the representations of the levels 0, 64 and the vectors representing other signal levels. B. Cross-validation accuracy of the VSA with dense distributed representations against the VSA with sparse distributed representations. A point corresponds to a dataset.

proposed approach requires the mapping of a feature value a_i to distributed representation \mathbf{F}_i (“value”) which preserve the similarity between nearby scalars. Kleyko et al. (2019) used thermometric encoding (Rachkovskij et al., 2005) to create such similarity preserving distributed representations. The feature set is represented as the sum of “key”-“value” pairs using the binding operation:

$$\mathbf{x} = f_{\kappa} \left(\sum_i^M \Phi_i \odot \mathbf{F}_i \right), \quad (23)$$

where f_{κ} denotes the clipping function which is used as a nonlinear activation function:

$$f_{\kappa}(x_i) = \begin{cases} -\kappa & x_i \leq -\kappa \\ x_i & -\kappa < x_i < \kappa \\ \kappa & x_i \geq \kappa \end{cases} \quad (24)$$

The clipping function is characterized by the configurable threshold parameter κ regulating nonlinear behavior of the neurons and limiting the range of activation values.

The predicted class \hat{y} is read out from \mathbf{x} using the trainable readout matrix as:

$$\hat{y} = \operatorname{argmax} \mathbf{W}^{\text{out}} \mathbf{x}, \quad (25)$$

where \mathbf{W}^{out} is obtained via the ridge regression applied to a training dataset.

For the purposes of using sparse block-codes, however, thermometric codes are non-sparse and their mean activity is variable across different values. Building on earlier efforts in the design of similarity-preserving sparse coding (Palm et al., 1994; Palm, 2013), we design a similarity-preserving encoding scheme with sparse block-codes. In this scheme, the lowest signal level has all hot components in the first positions of each block. The second signal level is encoded by the same pattern except that the hot component of the first block is shifted to the second position. The third signal level is encoded by the code of the second level with the hot component of the second block shifted to the second position, and so on. This feature encoding scheme can represent $N - K + 1$ signal levels uniquely. The similarity between vectors drops gradually as a function of distance

(Fig. 8A). Each pattern has the highest similarity with itself (overlap = K). For the range of distances between 1 and K , the overlap decreases linearly until it reaches 0 and then stays at this level for larger distances.

The data vectors in a classification problem are encoded by the following steps. First, labels of the different features (data dimensions) are encoded by random sparse block-code vectors. Key-value pairs are then formed by binding feature labels with corresponding values, using the similarity preserving sparse block-code scheme described above. A data vector is then represented by the sum of all the key-value pairs. In essence, such a representation coincides is a protected sum (5). In addition, we apply a clipping function to the resulting input.

The described representation of the data can be computed in a sparse block-code VSA, the last step can be represented by the activation of a hidden layer with nonlinear neurons. To perform classification, the hidden representation is pattern-matched to prototypes of the different classes. To optimize this pattern matching, in cases where the prototypes are correlated, we train a perceptron network with ridge regression, similar as previously proposed for in a sequence memory with VSAs (Fraday et al., 2018).

Interestingly, the cross-validated accuracies for VSAs with sparse block and dense representations (Kleyko et al., 2019) on 121 real-world classification datasets are quite similar (Fig. 8B), with a correlation coefficient of 0.88 and both reaching average accuracy of 0.80. The 121 datasets from the UCI Machine Learning Repository (Dua and Graff, 2019) have been initially analyzed in a large-scale comparison study of different classifiers (Fernandez-Delgado et al., 2014). The only preprocessing step we introduced was to normalize features in the range $[0, 1]$ and quantize the values into $N - K + 1$ levels. The hyperparameters for both dense and sparse models were optimized through grid search over N (for dense representations N varied in the range $[50, 1500]$ with step 50), λ (ridge regression regularization parameter; varied in the range $2^{[-10, 5]}$ with step 1), and κ (varied between $\{1, 3, 7, 15\}$). The search additionally considered K for sparse block-codes (K/N varied in the range $2^{[2, 5]}$ with step 1 while K varied in the range $2^{[4, 7]}$ with step 1).

Importantly, the average number of neurons used by both approaches was also comparable: about 500 for sparse block-codes and about 750 for dense representations. Thus, we conclude that sparse block-codes can be used as substitutes of dense representations for practical problems such as classifications tasks.

IV. DISCUSSION

In this paper we investigated methods for variable binding for symbolic reasoning with sparse distributed representations. The motivation for this study was two-fold. First, we believe that such methods of variable binding could be key for combining the universal reasoning properties of vector symbolic computing (Gayler, 2003) with advantages of neural networks. Second, these methods will enable implementations of symbolic reasoning that can leverage efficient sparse Hebbian associative

memories (Willshaw et al., 1969; Palm, 1980; Knoblauch and Palm, 2020) and low-power neuromorphic hardware (Davies et al., 2018).

A. Theoretical Results

Using the framework of compressed sensing, we investigated a setting in which there is a unique equivalence between sparse feature vectors and dense random vectors. We find that:

- i) With this setting, CS inference outperforms the classical VSA readout of set representations.
- ii) Classical vector symbolic binding between dense vectors with the Hadamard product (Plate, 2003; Gayler, 1998; Kanerva, 2009) is under certain conditions mathematically equivalent to tensor product binding (Smolensky, 1990) of the corresponding sparse vectors.
- iii) For representing sets of objects, vector addition of dense vectors (15) is equivalent to addition of the corresponding sparse vectors.
- iv) The protected sum of dense vectors (16) is equivalent to the concatenation of the sparse vectors.
- v) The dimensionality preserving operations between dense vectors for variable binding and protected set representations mathematically correspond to operations between sparse vectors, tensor product and vector concatenation, which are not dimensionality preserving.

B. Experimental Results

Our theory result v) implies that in order to construct dimensionality and sparsity-preserving variable binding between sparse vectors, an additional reduction step is required for mapping the outer product to a sparse vector. Existing reduction schemes of the outer product proposed in the literature, circular convolution (Plate, 2003) and vector-derived transformation binding (Gosmann and Eliasmith, 2019), are not sparsity-preserving when applied to sparse vectors.

For binding pairs of general K -sparse vectors, we designed a strategy of sub-sampling from the outer-product with additional thresholding to maintain sparsity. Such a computation can be implemented in neural circuitry where dendrites of neurons detect firing coincidences between pairs of input neurons. The necessary connection density increases with sparsity of the code vectors. Still, the computational complexity is order N when $K = \beta N$, which favorably compares to other binding operations which can have order of N^2 or $N \log N$. However, the sampling in the circuit always misses components of the tensor product, making the unbinding operation lossy.

Another direction we investigated extends previous work (Laiho et al., 2015) developing VSAs for sparse representations of restricted type, sparse block-codes. We propose block-wise circular convolution as a variable binding method which is sparsity and dimensionality preserving. Interestingly, for sparse block-codes, the unbinding given the reduced tensor and one of the factors is lossless. As our experiments show, it has the desired properties required for VSA manipulations, outperforming the other methods. Independent other work has proposed efficient Hebbian associative memory models (Kanter, 1988;

Gripon and Berrou, 2011; Knoblauch and Palm, 2020) that could be applied for cleanup steps required in VSAs with block-codes.

VSAs with block-codes are demonstrated in two applications. In a symbolic reasoning application we show that the accuracy as a function of the dimension of sparse block-codes reaches the full performance of dense VSAs and can be described by the same theory (Frady et al., 2018). On 121 classification datasets from the UCI Machine Learning Repository we show that the block-code VSA reaches the same performance as dense VSAs (Kleyko et al., 2019). Moreover, the average accuracy of 0.80 of VSAs models is comparable to the state-of-the-art performance of 0.82 achieved by Random Forest (Fernandez-Delgado et al., 2014).

C. Relationship to earlier work

Rachkovskij (2001); Rachkovskij and Kussul (2001) were to our knowledge the first to propose similarity- and sparsity-preserving variable binding. For binary representations they proposed methods that involve component-wise Boolean operations and deletion (thinning) based on random permutations. These methods of variable binding are also lossy, similar to our method of SPTP.

The variable binding with block-codes, which our experiments identify as the best, can be done with real-valued binary or complex-valued phasor block codes. For binary block-codes our binding method is the same as in (Laiho et al., 2015), who demonstrated it in a task processing symbolic sequences. For protecting individual elements in a sum representation, they use random permutations between blocks, rather than variable binding as we do in section III-A3.

D. Implications for neural networks and machine learning

In the deep network literature, concatenation is often used in neural network models as a variable binding operation (Soll et al., 2019). However, our result iv) suggests that concatenation is fundamentally different from a binding operation. This might be a reason why deep learning methods have limited capabilities to represent and manipulate data structures (Marcus, 2020).

Several recent studies have applied VSAs to classification problems (Ge and Parhi, 2020; Rahimi et al., 2019). Here we demonstrated classification in a block-code VSA. The block-code VSA exhibited the same average classification accuracy as earlier VSA solutions with dense codes. This result suggests that sparse block-code VSAs can be a promising basis for developing classification algorithms for low-power neuromorphic hardware platforms (Davies et al., 2018).

E. Implications for neuroscience

We have investigated variable binding operations between sparse patterns regarding their computational properties in symbolic reasoning. It is interesting that this form of variable binding requires multiplication or coincidence detection, computations which can be implemented by active dendritic mechanisms of biological neurons (Larkum and Nevian, 2008). Although this computation is beyond the capabilities of standard neural

networks, it can be implemented with formal models of neurons, such as sigma-pi neurons (Mel and Koch, 1990).

We found that the most efficient form of variable binding with sparse vectors relies on block-code structure. Although block-codes were engineered independent of neurobiology, they compatible with some experimental observations, such as divisive normalization (Heeger, 1992), and functional modularity. Specifically, in sensory cortices of carnivores neurons within small cortical columns (Mountcastle, 1957) respond to the same stimulus features, such as the orientation of local edges in the image (Hubel and Wiesel, 1963, 1977). Further, groups of nearby orientation columns form so-called macro columns, tiling all possible edge orientations at a specific image location (Hubel and Wiesel, 1974; Swindale, 1990). A macro column may correspond to a block in a block-code.

While binary block-codes are not biologically plausible, complex-valued block-codes in which active elements are complex phasors with unit magnitude, can be represented as timing patterns in networks of spiking neurons (Frady and Sommer, 2019). Further, it seems possible to extend LCC binding to soft block-codes, in which localized bumps with graded neural activities represented by spike rate, e.g. (Ben-Yishai et al., 1995).

F. Future directions

One important future direction is to investigate how to combine the advantages of VSA and traditional neural networks to build more powerful tools for artificial intelligence. The challenge is how to design neural networks for learning sparse representations that can be processed in sparse VSAs. Such combined systems could potentially overcome some of the severe limitations of current neural networks, such as the demand of large amounts of data, limited abilities to generalize learned knowledge, etc.

Another interesting research direction is to design VSAs operating with spatio-temporal spike patterns that can be implemented in neuromorphic hardware, potentially also making use spike timing and efficient associative memory for spike timing patterns (Frady and Sommer, 2019).

Further, it will be interesting to study how binding in sparse VSAs can be used to form similarity-preserving sparse codes (Palm et al., 1994; Palm, 2013) for continuous manifolds. For example, binding can be used to create index patterns for representing locations in space, which could be useful for navigation in normative modeling of hippocampus (Frady and Sommer, 2020).

ACKNOWLEDGEMENT

The authors thank Charles Garfinkle and other members of the Redwood Center for Theoretical Neuroscience for stimulating discussions. DK is supported by the European Unions Horizon 2020 research and innovation programme under the Marie Skłodowska-Curie Individual Fellowship grant agreement No. 839179, and DARPA’s VIP program under Super-HD project. FTS is supported by NIH R01-EB026955.

APPENDIX A

RELATIONS BETWEEN DIFFERENT VARIABLE BINDING OPERATIONS

A. VSA binding, a subsampling of TRP

The dimensionality-preserving binding operations in VSAs can be expressed as a sampling of the tensor product matrix $\mathbf{x} \mathbf{y}^\top$ into a vector:

$$\mathbf{x} \circ \mathbf{y} = \sum_{ij} W_{ij}^l x_i y_j \quad (26)$$

where the binary third-order tensor $\mathbf{W} \in \{0, 1\}^{N \times N \times N}$ determines what elements of the outer-product are sampled. For the Hadamard product in the MAP VSA, the sampling tensor just copies the diagonal elements of the tensor matrix into a vector, using a sampling tensor $W_{ij}^l = \delta(i, j)\delta(i, l)$. Here $\delta(i, j)$ is the Kronecker symbol. Conversely, in circular convolution the sampling involves summing the diagonals of the outer-product matrix:

$$W_{ij}^l = \delta((i + l - 1) \bmod n, j) \quad (27)$$

For neurally implementing a binding operation, like (17), a low fan-in is essential. The *fan-in* is the number of nonzero elements in the tensor feeding the coincidences between the input vectors to an output neuron $\alpha = \alpha(l) = \sum_{ij} W_{ij}^l$. For circular convolution the fan-in is $\alpha_{CCB} = N$. For VDTB binding the fan-in is $\alpha_{VDTB} = \sqrt{N}$. When applied to a pair of sparse vectors, circular convolution and VDTB binding are not sparsity-preserving. In the next section we analyze the properties of the sampling tensor (26) required to make (17) a sparsity-preserving binding operation for general K -sparse vectors with optimal properties.

B. Generalizing the Fourier Convolution Theorem

There is a direct relation between circular convolution binding and the Hadamard product binding through the Fourier convolution theorem. The Fourier transform is a (non-random) linear transform that previously has been proposed in holography for generating (dense) distributed representations from data features. The *Fourier convolution theorem* states:

$$\mathcal{F}(\mathbf{a}) \odot \mathcal{F}(\mathbf{b}) = \mathcal{F}(\mathbf{a} * \mathbf{b}) \quad (28)$$

where $\mathcal{F}(z) := (1/n) \sum_{m=0}^{n-1} \Phi_{-km}^F z_m$ with $\Phi_{km}^F := e^{j \frac{2\pi km}{n}}$ is the discrete Fourier transform. With (26) and (27), the Fourier convolution theorem establishes a relationship between the outer product of two vectors and the Hadamard product of their Fourier transforms. Replacing the Fourier transform by two CS random sampling matrices, the Fourier convolution theorem generalizes to:

$$\Phi \mathbf{a} \odot \Psi \mathbf{b} = \mathcal{J}(\mathbf{a} \mathbf{b}^\top) \quad (29)$$

This equation coincides with (13), describing the relationship between the Hadamard product of dense vectors to the outer product of the corresponding sparse vectors. The linear projection \mathcal{J} is formed from the CS sampling matrices Φ and Ψ . Note, that there is no general invertibility of \mathcal{J} , unlike in the Fourier convolution theorem. The outer product of the sparse vectors can

be uniquely inferred from the Hadamard product of the dense vectors under certain conditions of sparsity, dimensionality, and properties of the sampling matrices, as discussed in Sect. III-A2.

APPENDIX B

SPARSITY-PRESERVING BINDING FOR K -SPARSE VECTORS

A. Analysis of required fan-in

We examine the required fan-in in (17) for two types of random sampling tensors for sparsity-preserving binding (Fig. 4). One type in which the tensor product of the input vectors is sampled entirely randomly with a fixed constant fan-in per downstream neuron. And another type, in which the tensor is sampled along its diagonals, similar to circular convolution, but the diagonals truncated by a fixed sized fan-in of the downstream neurons.

First, we determine the minimal fan-in that still provides signals at downstream neurons so that a threshold operation can reliably produce a K -sparse vector. The dendritic sums in (17) are approximately distributed by the following Binomial distribution:

$$p(d_l = r) = \binom{\alpha}{r} \left(\frac{K^2}{N^2}\right)^r \left(1 - \frac{K^2}{N^2}\right)^{\alpha-r} \quad (30)$$

We require that the fan-in is large enough so that the expected number of downstream neurons with $d_l = 0$ is smaller than the number of silent neurons in the K -sparse result vector: $Np(d_l = 0) < N - K$. To satisfy this condition, a lower bound α^* to the minimal fan-in is computed, which ensures the equality between the two numbers and translates into the condition that for a threshold of $\theta = 1$ the patterns sparsity is preserved:

$$p(d_l = 0) \stackrel{!}{=} 1 - \frac{K}{N} \quad (31)$$

Inserting (30) into this condition we obtain after some algebra:

$$\alpha > \alpha^* = \frac{\ln\left(1 - \frac{K}{N}\right)}{\ln\left(1 - \frac{K^2}{N^2}\right)} \quad (32)$$

For sparse patterns, (32) becomes simply $\alpha^* = N/K$.

Note, that setting the fan-in exactly to the lower bound α^* should result in patterns of dendritic activity in the population of downstream neurons which are approximately K -sparse, without any thresholding necessary. One can generalize condition (31) to an arbitrary threshold:

$$\begin{aligned} \sum_{i=0}^{\theta-1} p(d_l = i) &= (\alpha - \theta + 1) \binom{\alpha}{\theta - 1} \int_0^{1 - \frac{K^2}{N^2}} t^{\alpha-\theta} (1-t)^{\theta-1} dt \\ &\stackrel{!}{=} 1 - \frac{K}{N} \end{aligned} \quad (33)$$

Unfortunately, the variable α cannot be analytically resolved from the exact condition (33). However, it is straight-forward to compute α numerically (Fig. 9A).

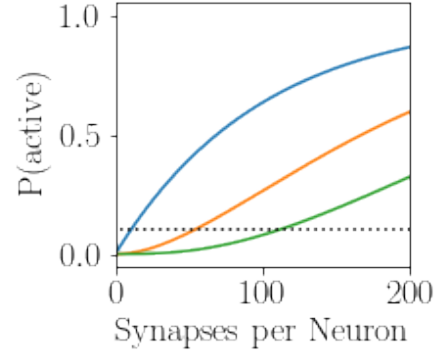


Fig. 9. **Fan-in requirements of SPTP.** The fan-in for each neuron can be determined from the binomial distribution. Higher thresholds require more fan-in ($\theta = [1, 2, 3]$). The fan-in is determined where each colored line crosses the sparsity level (black line shows 10% sparsity).

B. Symmetry for optimizing unbinding performance

Another crucial question is what symmetry of the \mathbf{W} tensor best enables the invertibility of the sparsity-preserving binding operation (17). Chaining a binding and unbinding step, one obtains the following self-consistency condition:

$$a_i = H \left(\sum_{j,l} W_{jl}^i b_j H \left(\sum_{i',j'} W_{i'j'}^l a_{i'} b_{j'} - \theta \right) - \theta \right) \quad (34)$$

which should hold for arbitrary K -sparse vectors \mathbf{a} and \mathbf{b} . The self-consistency condition can be approximately substituted by maximizing the objective function $\mathcal{L} := \sum_i a_i (d_i - \theta)$. Replacing also the inner nonlinearity by its argument we obtain:

$$\begin{aligned} \mathcal{L}(W_{jl}^i; \mathbf{a}, \mathbf{b}, \theta) &= \sum_{i,j,i',j'} W_{ij}^i W_{i'j'}^l a_i a_{i'} b_j b_{j'} \\ &\quad - \theta \left(\sum_{ijl} W_{jl}^i a_i b_j + K \right) \end{aligned} \quad (35)$$

The quantity (35) should be high for any vectors \mathbf{a}, \mathbf{b} . Thus it is only the expectation (over all vectors \mathbf{a} and \mathbf{b}) of first term that can be consistently increased by changing the structure of the sampling tensor. The biggest increase is achieved by making sure that terms with $(a_i)^2 (b_j)^2$ are zeroed out with probability $1 - \alpha$ rather than with $1 - \alpha^2$, which can be accomplished by introducing the following symmetry into the sampling tensor:

$$W_{jl}^i = W_{ij}^l \quad (36)$$

For sparse complex vectors one can define a binding operation with the nonlinearity $f_\Theta(x) = \frac{x}{|x|} H(|x| - \Theta)$ taken from (Fraday and Sommer, 2019):

$$\mathbf{a} \circ \mathbf{b} = f_\Theta \left(\sum_{jl} W_{ij}^l a_i b_j \right) \quad (37)$$

where the sampling tensor is binary random or a random phasor tensor. The corresponding selfconsistency condition is then:

$$a_i = f_{\Theta} \left(\sum_{j,l} W_{jl}^i \bar{b}_j f_{\Theta} \left(\sum_{i',j'} W_{i'j'}^l a_{i'} b_{j'} \right) \right) \quad (38)$$

$$\simeq f_{\Theta} \left(\sum_{j,l,i',j'} W_{jl}^i W_{i'j'}^l a_{i'} b_{j'} \bar{b}_j \right)$$

In (38) one can notice that the signal is maximized if the tensor fulfills the following symmetry:

$$W_{jl}^i = \bar{W}_{ij}^l \quad (39)$$

Even with condition (39) the unbinding will be noisy and cleanup through an additional associative network will be required.

REFERENCES

- Amini, A. and Marvasti, F. (2011). Deterministic construction of binary, bipolar, and ternary compressed sensing matrices. *IEEE Transactions on Information Theory*, 57(4):2360–2370.
- Bell, A. J. and Sejnowski, T. J. (1997). The independent components of natural scenes are edge filters. *Vision research*, 37(23):3327–3338.
- Ben-Yishai, R., Bar-Or, R. L., and Sompolinsky, H. (1995). Theory of orientation tuning in visual cortex. *Proceedings of the National Academy of Sciences*, 92(9):3844–3848.
- Candes, E. J., Romberg, J. K., and Tao, T. (2006). Stable signal recovery from incomplete and inaccurate measurements. *Communications on Pure and Applied Mathematics: A Journal Issued by the Courant Institute of Mathematical Sciences*, 59(8):1207–1223.
- Davies, M., Srinivasa, N., Lin, T. H., Chinya, G., Cao, Y., Choday, S. H., Dimou, G., Joshi, P., Imam, N., Jain, S., Liao, Y., Lin, C. K., Lines, A., Liu, R., Mathaikutty, D., McCoy, S., Paul, A., Tse, J., Venkataramanan, G., Weng, Y. H., Wild, A., Yang, Y., and Wang, H. (2018). Loihi: A Neuromorphic Manycore Processor with On-Chip Learning. *IEEE Micro*, 38(1):82–99.
- Donoho, D. L. et al. (2006). Compressed sensing. *IEEE Transactions on information theory*, 52(4):1289–1306.
- Dua, D. and Graff, C. (2019). UCI machine learning repository.
- Eldar, Y. C., Kuppinger, P., and Bolcskei, H. (2010). Block-sparse signals: Uncertainty relations and efficient recovery. *IEEE Transactions on Signal Processing*, 58(6):3042–3054.
- Fernandez-Delgado, M., Cernadas, E., Barro, S., and Amorim, D. (2014). Do we need hundreds of classifiers to solve real world classification problems? *Journal of Machine Learning Research*, 15:3133–3181.
- Fodor, J. A., Pylyshyn, Z. W., et al. (1988). Connectionism and cognitive architecture: A critical analysis. *Cognition*, 28(1-2):3–71.
- Frady, E. P., Kleyko, D., and Sommer, F. T. (2018). A theory of sequence indexing and working memory in recurrent neural networks. *Neural Computation*, 30(6):1449–1513.
- Frady, E. P. and Sommer, F. T. (2019). Robust computation with rhythmic spike patterns. *PNAS*, 116(36):18050–18059.
- Frady, E. P. and Sommer, F. T. (2020). A normative hippocampus model: robustly encoding variables on smooth manifolds using spiking neurons. In *2020 Proceedings*, page 221. CoSyNe.
- G. Huang and Q. Zhu and C. Siew (2006). Extreme learning machine: Theory and applications. *Neurocomputing*, 70(1-3):489–501.
- Ganguli, S. and Sompolinsky, H. (2010). Statistical mechanics of compressed sensing. *Physical Review Letters*, 104(18):1–4.
- Gayler, R. W. (1998). Multiplicative binding, representation operators & analogy. In *Gentner, D., Holyoak, K. J., Kokinov, B. N. (Eds.), Advances in analogy research: Integration of theory and data from the cognitive, computational, and neural sciences*, pages 1–4, New Bulgarian University, Sofia, Bulgaria.
- Gayler, R. W. (2003). Vector Symbolic Architectures answer Jackendoff’s challenges for cognitive neuroscience. *Proceedings of the ICCS/ASCS International Conference on Cognitive Science*, (2002):6.
- Ge, L. and Parhi, K. K. (2020). Classification using Hyperdimensional Computing: A Review. *arXiv:2004.11204*, pages 1–16.
- Gosmann, J. and Eliasmith, C. (2019). Vector-derived transformation binding: An improved binding operation for deep symbol-like processing in neural networks. *Neural computation*, 31(5):849–869.
- Gripon, V. and Berrou, C. (2011). Sparse neural networks with large learning diversity. *IEEE transactions on neural networks*, 22(7):1087–1096.
- Gritsenko, V., Rachkovskij, D., Frolov, A., Gayler, R., Kleyko, D., and Osipov, E. (2017). Neural distributed autoassociative memories: A survey. *Cybernetics and Computer Engineering*, 2(188):5–35.
- Heeger, D. J. (1992). Normalization of cell responses in cat striate cortex. *Visual neuroscience*, 9(2):181–197.
- Hillar, C. J. and Sommer, F. T. (2015). When can dictionary learning uniquely recover sparse data from subsamples? *IEEE Transactions on Information Theory*, 61(11):6290–6297.
- Hinton, G. E. (1990). Mapping part-whole hierarchies into connectionist networks. *Artificial Intelligence*, (46):47–76.
- Hinton, G. E. et al. (1986). Learning distributed representations of concepts. In *Proceedings of the eighth annual conference of the cognitive science society*, volume 1, page 12. Amherst, MA.
- Hinton, G. E., McClelland, J. L., and Rumelhart, D. E. (1990). Distributed representations. *The philosophy of artificial intelligence*, pages 248–280.
- Hopfield, J. J. (1982). Neural networks and physical systems with emergent collective computational abilities. *Proceedings of the National Academy of Sciences of the United States of America*, 79(8):2554–2558.
- Hubel, D. H. and Wiesel, T. (1963). Shape and arrangement of columns in cat’s striate cortex. *The Journal of physiology*, 165(3):559–568.
- Hubel, D. H. and Wiesel, T. N. (1974). Sequence regularity and geometry of orientation columns in the monkey striate

- cortex. *Journal of Comparative Neurology*, 158(3):267–293.
- Hubel, D. H. and Wiesel, T. N. (1977). Ferrier lecture-functional architecture of macaque monkey visual cortex. *Proceedings of the Royal Society of London. Series B. Biological Sciences*, 198(1130):1–59.
- Igel'nik, B. and Pao, Y. (1995). Stochastic choice of basis functions in adaptive function approximation and the functional-link net. *IEEE Transactions on Neural Networks*, 6:1320–1329.
- Kanerva, P. (1996). Binary spatter-coding of ordered K-tuples. *Lecture Notes in Computer Science (including subseries Lecture Notes in Artificial Intelligence and Lecture Notes in Bioinformatics)*, 1112 LNCS:869–873.
- Kanerva, P. (2009). Hyperdimensional computing: An introduction to computing in distributed representation with high-dimensional random vectors. *Cognitive Computation*, 1:139–159.
- Kanerva, P. (2010). What We Mean When We Say “What’s the Dollar of Mexico?”: Prototypes and Mapping in Concept Space. In *AAAI Fall Symposium: Quantum Informatics for Cognitive, Social, and Semantic Processes*, pages 2–6.
- Kanter, I. (1988). Potts-glass models of neural networks. *Physical Review A*, 37(7):2739–2742.
- Kleyko, D., Kheffache, M., Frady, E. P., Wiklund, U., and Osipov, E. (2019). Density encoding enables resource-efficient randomly connected neural networks. *arXiv:1909.09153*, pages 1–7.
- Knoblauch, G. E. and Palm, G. (2020). Iterative retrieval and block coding in auto- and hetero-associative memory. *Neural Computation*, 32(1):205–260.
- Laiho, M., Poikonen, J. H., Kanerva, P., and Lehtonen, E. (2015). High-dimensional computing with sparse vectors. *2015 IEEE Biomedical Circuits and Systems Conference (BioCAS)*, pages 1–4.
- Larkum, M. E. and Nevian, T. (2008). Synaptic clustering by dendritic signalling mechanisms. *Current opinion in neurobiology*, 18(3):321–331.
- Ledoux, M. (2001). *The concentration of measure phenomenon*. Number 89. American Mathematical Soc.
- Marcus, G. (2020). The Next Decade in AI: Four Steps Towards Robust Artificial Intelligence. *arXiv:2002.06177*, pages 1–59.
- Mel, B. W. and Koch, C. (1990). Sigma-pi learning: On radial basis functions and cortical associative learning. In *Advances in neural information processing systems*, pages 474–481.
- Mountcastle, V. B. (1957). Modality and topographic properties of single neurons of cat’s somatic sensory cortex. *Journal of neurophysiology*, 20(4):408–434.
- Olshausen, B. A. and Field, D. J. (1996). Natural image statistics and efficient coding. *Network (Bristol, England)*, 7(2):333–9.
- Palm, G. (1980). On associative memory. *Biological cybernetics*, 36(1):19–31.
- Palm, G. (2013). Neural associative memories and sparse coding. *Neural Networks*, 37:165–171.
- Palm, G., Schwenker, F., and Sommer, F. T. (1994). Associative memory networks and sparse similarity preserving codes. In *From Statistics to Neural Networks*, pages 282–302. Springer.
- Palm, G. and Sommer, F. T. (1992). Information capacity in recurrent mcculloch–pitts networks with sparsely coded memory states. *Network: Computation in Neural Systems*, 3(2):177–186.
- Plate, T. A. (1991). Holographic Reduced Representations : Convolution Algebra for Compositional Distributed Representations. *Proceedings of the 12th international joint conference on Artificial intelligence*, pages 30–35.
- Plate, T. A. (1993). Holographic Recurrent Networks. *Advances in Neural Information Processing Systems*, 5(1):34–41.
- Plate, T. A. (1994). *Distributed Representations and Nested Compositional Structure*. PhD thesis.
- Plate, T. A. (2003). *Holographic Reduced Representation: Distributed Representation for Cognitive Structures*. Stanford: CSLI Publications.
- Plate, T. A. T. (1995). Holographic reduced representations. *IEEE Transactions on Neural Networks*, 6(3):623–641.
- Rachkovskij, D. A. (2001). Representation and processing of structures with binary sparse distributed codes. *IEEE Transactions on Knowledge and Data Engineering*, 13(2):261–276.
- Rachkovskij, D. A. and Kussul, E. M. (2001). Binding and Normalization of Binary Sparse Distributed Representations by Context-Dependent Thinning. *Neural Computation*, 13(2):411–452.
- Rachkovskij, D. A., Slipchenko, S. V., Kussul, E. M., and Baidyk, T. N. (2005). Sparse binary distributed encoding of scalars. *Journal of Automation and Information Sciences*, 37(6):12–23.
- Rahimi, A., Kanerva, P., Benini, L., and Rabaey, J. M. (2019). Efficient biosignal processing using hyperdimensional computing: Network templates for combined learning and classification of ExG signals. *Proceedings of the IEEE*, 107(1):123–143.
- Scardapane, S. and Wang, D. (2017). Randomness in neural networks: An overview. *Data Mining and Knowledge Discovery*, 7:1–18.
- Smolensky, P. (1990). Tensor product variable binding and the representation of symbolic structures in connectionist systems. *Artificial Intelligence*, 46(1-2):159–216.
- Smolensky, P., Lee, M., He, X., Yih, W.-t., Gao, J., and Deng, L. (2016). Basic reasoning with tensor product representations. *arXiv preprint arXiv:1601.02745*.
- Soll, M., Hinz, T., Magg, S., and Wermter, S. (2019). Evaluating defensive distillation for defending text processing neural networks against adversarial examples. In *International Conference on Artificial Neural Networks (ICANN)*, pages 685–696. Springer.
- Swindale, N. V. (1990). Is the cerebral cortex modular? *Trends in Neurosciences*, 13(12):487–492.
- Treisman, A. (1998). Feature binding, attention and object perception. *Philosophical Transactions of the Royal Society of London. Series B: Biological Sciences*, 353(1373):1295–1306.
- Tsodyks, M. V. and Feigel’man, M. V. (1988). The enhanced storage capacity in neural networks with low activity level. *Europhysics Letters*, 6(2):101–105.

Willshaw, D. J., Buneman, O. P., and Longuet-Higgins, H. C. (1969). Non-holographic associative memory. *Nature*.